Insight - Physics 2024, 7(1), 641.
https://doi.org/10.18282/ip641

Article

Strong-field nondipole approximation in laser-assisted thermal electron scattering

Chiranjibi Shrestha[1], Saddam Husain Dhobi[1,2,*], Narayan Babu Shrestha[3]

[1] Central Department of Physics, Tribhuvan University, Kathmandu 46000, Nepal
[2] Physical Science Unit, Nepal Academy of Science and Technology, Lalitpur 44700, Nepal
[3] Department of Physics, Patan Multiple Campus, Tribhuvan University, Lalitpur 44700, Nepal
*** Corresponding author:** Saddam Husain Dhobi, saddam@ran.edu.np

CITATION

Shrestha C, Dhobi SH, Shrestha NB. Strong-field nondipole approximation in laser-assisted thermal electron scattering. Insight - Physics. 2024; 7(1): 641. https://doi.org/10.18282/ip641

ARTICLE INFO

Received: 31 July 2023
Accepted: 10 September 2024
Available online: 20 November 2024

Abstract: This study investigates the differential cross-section (DCS) of electrons scattered by a hydrogen molecule (H_2) under varying conditions, including temperature, momentum, laser intensity, and polarization. The objective was to understand how these parameters affect electron scattering and to compare the effects of linear and circular polarizations. Methodologically, theoretical model was developed using strong-field nondipole approximation with linear and circular polarized laser fields, examining DCS as a function of thermal electron temperature, momentum, and laser intensity. The study utilized a modified Volkov wave function model to account for thermal electron effects and analyzed DCS variations across different orbitals ($n = 1$, $n = 2$, and $n = 3$). Findings reveal that DCS increases with temperature due to enhanced electron oscillations, with higher orbitals ($n = 3$) showing greater DCS compared to lower orbitals ($n = 1$). Increased momentum results in decreased DCS, with higher orbitals exhibiting higher DCS values under circular polarization, contrary to linear polarization. Laser intensity decreases DCS for both polarizations, with circular polarization providing a narrower range of DCS values and generally higher DCS compared to linear polarization. This research further exploration of polarization effects on DCS in different atomic systems and extending studies to higher energy regions for a comprehensive understanding of electron scattering dynamics.

Keywords: differential cross-section; laser-assisted scattering; nondipole strong-field approximation; thermal electron effects; polarization effects

1. Introduction

Various theoretical techniques and advances in the study of electron-photon interactions, especially in the presence of strong electromagnetic fields [1]. The effect of background potentials on electron-photon scattering is also investigated, with cross-sectional expressions produced for different levels of laser illumination [2]. In addition, Kroll and Watson [3] describe a practical approximation for multiphoton energy-transfer methods in the presence of a scattering potential as well as powerful external electromagnetic fields. Understanding multiphoton events through a unitary transformation approach, which simplifies the consideration of multiphoton transitions and ionisations in many-electron atoms [4]. Bergou [5] introduces a perturbative method for analysing intense field issues and estimating bremsstrahlung cross sections, as well as accurate solutions to the Dirac equation that provide insights into nonlinear Compton scattering. More recent research has emphasised systematic methods for analysing multiphoton events in atomic physics, including both perturbative as well as non-perturbative approaches, to meet issues provided by high

field strengths, intermediate resonances, particularly finite pulse durations [6]. The study also discusses advances in understanding electron-atom collisions in laser fields, emphasising approximation approaches and the incorporation of atomic structure into theoretical treatments [7]. Finally, novel approaches for reaching high temporal resolution in gas electron diffraction including the potential for increased electron conductance in semiconductors under intense infrared electromagnetic fields are reviewed [8,9].

Laser-matter interactions can be categorized into different regimes. Strong-field physics primarily deals with interactions in the nonrelativistic regime, where the laser field's strength is comparable to the forces binding electrons within atoms. High-field physics considers the laser field as a propagating electromagnetic wave, accounting for both its temporal and spatial variations. Traditionally, non-dipole phenomena in photoionisation have been thought to be minimal from the infrared region to the soft X-ray domains, with earlier studies limited to single-pulse, single-color data. Yet, attosecond time-resolved spectroscopy was recently extended to the non-dipole interaction regime. Researchers used self-referenced attosecond photoelectron interferometry upon helium atoms to determine electron sub cycle mobility along the light propagation direction throughout the 15 pm range, which was controlled by a near-infrared laser field's magnetic component. They detected a temporal delay of 15 ± 10 attoseconds during the electric-dipole along with electric-quadrupole transitions by resolving the asymmetry of photoelectron forward-backward yielding with attosecond accuracy. These conclusions are supported by ab initio calculations using the non-dipole time-dependent Schrödinger equation [10].

Böning et al. [11] investigated the nondipole strong-field approximation (SFA) with spatially structured laser fields and discovered that it is commonly used to theoretically describe the ionisation of molecules and atoms in intense laser fields. They derive Volkov-type continuous wave functions involving an electron travelling in a laser field with arbitrary spatial dependency. Building on Rosenberg and Zhou's [12] work, they demonstrate how to create Volkov-type solutions that solve the Schrödinger equation involving an electron in the vector form potential which can be expressed as an integrated superposition over plane waves. These solutions are not limited to plane waves; they may also be applied to more complicated laser fields, where the magnetic field is crucial, like twisting Bessel or Laguerre-Gaussian beams. For circular polarisation, they find strong agreement with earlier theoretical and experimental research; for linear polarisation, they explore differences; however, they do not take thermal electrons into account for scattering. We take into account the heat environment, which ranges from 15 °C to 200 °C, as an external component in this work [12].

High-sensitivity electron emission spectra for xenon in a powerful 50 ps, 1.053 μm laser beam. Unlike the severe cutoff seen in xenon optical harmonics generation spectra, the above-threshold ionisation distribution steadily drops over the whole energy spectrum range (0–30 eV) with no sudden shifts in slope. The unresolved link between electron along with photon emission from an atom under an intense field is directly addressed by the calculations employing the single present electron approximation, which yields excellent agreement regarding the measured electron distribution [13].

Our comprehension of materials' electrical reaction to applied intense laser beams is challenged by their rapid dynamics. With their highly adjustable potentials, trapped ultracold atoms have grown into an enabling tool for understanding phenomena where certain effects are 12 orders magnitude slower but more readily accessible. The mapping of atto-science platform parameters to atomic cloud simulations and the proposal of an experimental technique to reach the high-harmonic generation emission spectrum—a regime that has proven difficult for cold-atom simulation to simulate thus far—will allow for further research. The effectiveness of both short and extended nuclear potentials, as well as how they react to ultrashort few-cycle pulses or applied elliptically polarised fields [14]. The phase for high-order harmonics generated when powerful laser pulses interact with atoms. A finite using closed analytic formula is obtained by aligning the initially diverging Coulomb integral into the phases that comprise the atomic wave function at ionisation and recombination using a calculation based on the formalism with quantum orbits as well as the imaginary time technique. The yield as well as the interference pattern of high harmonic spectra can be considerably altered by using complex-valued Coulomb phase [15].

Quantum tunnelling between merging nuclei when a time-varying harmonic field is present. Floquet/Volkov (FV) as well as Kramers-Henneberger (KH) methods are used to compute the tunnelling rate, and both are compared to a Crank-Nicolson (CN) type first-principles numerical solution. The FV approach's usage in analytical estimations of laser-enhanced reactivity is justified by numerical validation, whereas the KH approach is unable to replicate the other approaches' predictions. Significant improvement of fusion reactivity for a deuterium-tritium plasma at 1 keV temperature requires field strengths of order 10^{15}–10^{16} V/m and photon energies below 1 keV, which are within the reach of next-generation x-rays free electron lasers (XFELs) [16]. For phonons close to the edge of the Brillouin zone, there is a brief increase in their population on an interval of about 1 picosecond, caused by strong electron-phonon interaction, and a gradual decline on a timescale of about 8 picoseconds, controlled by weaker phonon-phonon relaxing. The two processes are separated by tungsten's remarkable harmonicity, which produces long-lived nonequilibrium phonons for a pure metal. This result emphasises that the phonon thermal propagation of metals may be determined by electron-phonon scattering [17].

The periodic changes of plasma characteristics in filament plasmas are measured via Thomson scattering. Important aspects of precise measurement are also covered, including plasma emission, stray light attenuation, as well as alignment. Two perpendicular overlapping laser pulses are used in the setup: a femtosecond laser for creating the plasma filament and a nanosecond probe beam. The temporal variation of the electron density in the nitrogen filament at 1 atm can be observed by varying their relative delay. Excellent quantitative agreement is seen between the data and simulations on the temporal motion of electrons. Finally, it is demonstrated that filament emission has a major influence on the estimate of the electron number density [18]. Thermal effects on the scattering of electrons were not taken into account in earlier studies, despite a great deal of research. We fill this gap in this work by taking into account the effects of thermal settings with temperatures that vary from 15 °C–200 °C on thermal electron scattering.

2. Materials and methods

We developed a high-intensity laser-matter interaction setup capable of investigating both strong-field and high-field regimes, utilizing a tunable laser source that delivers ultra-short, high-intensity pulses and supports various polarizations including linear, circular, and twisted beams. Our system incorporates advanced computational models with modified Volkov wave functions to account for thermal electrons, enabling the calculation of DCS under laser influence. This setup enhances our understanding of electron behaviors and quantum phenomena in extreme conditions. An electron obeys the dependent on time Schrödinger equation in an outside electromagnetic radiation field along with vector potential A(r, t) [12],

$$i\frac{\partial}{\partial t}\chi(r,t) = \frac{1}{2}[\mathrm{p} + e\mathrm{A}(r,t)]^2\chi(r,t) \tag{1}$$

The momentum operator in this case is denoted by p, while the electromagnetic field's vector potential is represented by A(r, t). This equation is a version of the dependent on time Schrödinger equation, in which the interaction between the momentum of the particle with the external electromagnetic radiation is incorporated by the expression $[\mathrm{p} + \mathrm{eA(r, t)}]^2$. Applications of this formulation include the study of processes like the quantum Hall effect as well as the behaviour of electrons within a magnetic field, as well as the analysis of charged particles' behaviour in variable electromagnetic fields—an important area in quantum mechanics and solid-state physics. In this situation, the vector potential A(t) is uniform in space and fluctuates with time, similar to the behaviour associated with a monochromatic electromagnetic wave using the dipole approximation.

$$\chi_{\mathrm{p}}(r,t) = \frac{1}{(2\pi)^{\frac{3}{2}}}e^{i\phi(r,t)} = \frac{1}{(2\pi)^{\frac{3}{2}}}e^{i\left(\mathrm{p.r}-\frac{p^2}{2}t\right)} \tag{2}$$

In particular, the dipole approximation used under thermal conditions yields solutions that solve the time-dependent Schrödinger Equation (1) for monochromatic along with time-dependent light fields, A(t) ≠ A(r, t) [19]. When analysing a particle's behaviour under the impact of an exterior time-dependent electromagnetic field, like a laser, the time-dependent Schrödinger equations under this circumstance is utilised. We can treat the applied field as being uniform over the particle's whole spatial extent since the dipole approximation implies because the wavelength of the generated field is significantly bigger than the system's size.

$$\chi_{\mathrm{p}}(r,t) = \frac{1}{(2\pi)^{\frac{3}{2}}}e^{i\mathrm{p.r}}e^{-iS_{\mathrm{V}}(t)} - \mathrm{k_e}\nabla\mathrm{T}\exp(\mathrm{i}\omega_T t) \tag{3}$$

These solutions are referred to as Volkov states and describe electrons with an established kinetic momentum *p* [20]. Initially, Rosenberg and Zhou [21] derived these solutions for a limited set of discrete laser modes, including those with nonparallel wave vectors *k*. We have extended this work to encompass continuous superpositions of laser modes, allowing for the incorporation of various spatial profiles incorporating the driving beam into the photoelectron's quantum dynamics, such as Gaussian as well as twisted light beams [22]. This generalization often involves complex integrals. The

Volkov solutions can be expressed using a modified Volkov phase Γ(r, t).

$$\chi_{\mathrm{p}}(r,t)=\frac{1}{(2\pi)^{\frac{3}{2}}}e^{i\left(\mathrm{p.r}-\frac{p^2}{2}t\right)}\,e^{-i\Gamma(r,t)}-\mathrm{k_e}\nabla\mathrm{T}\exp(\mathrm{i}\omega_{\mathrm{T}}\mathrm{t}) \tag{4}$$

where, $\Gamma(r,t)=\Gamma_1(r,t)+\Gamma_2(r,t)+\Gamma_3(r,t)+\mathrm{O}\left(\frac{\beta_0^{\frac{3}{2}}}{a_0\lambda^{\frac{1}{2}}}\right)$ this is the result of the free electron interacting with different elements of the vector potential, and which is composed of three contributions, $\Gamma_{\mathrm{i}}(r,t)$, i = 1, 2, 3 [23]. Our method, in contrast to other research, includes arbitrary integral a superposition of plane-wave modes in addition to discrete superpositions. A vector potential for linear plans of the kind is what we start with.

$$\mathrm{A}(r,\mathrm{t})=\int d^3k\,\mathrm{A}(k,\mathrm{t}) \tag{5}$$

where $A(k,\mathrm{t})=Re\{a(k)e^{iu_k}\}$, with wave vectors, complicated and a(k) Fourier coefficients. As a shorthand to describe the time-harmonic phase associated with the plane-wave component of the laser field, we use $u_k = u_k$(r, t) = $kr - \omega_k t$ using $\omega_k = k_c$. and $a(k)=A_0e_x\delta(k-k_0)$. Also, we have $\Gamma(r,t)=\rho_L\sin(u_{k_0})+\alpha_L\sin(2u_{k_0})+2\alpha_L u_{k_0}$with $\alpha_L=\frac{A_0^2}{8\eta_{k_0}},\rho_L=\frac{A_0p_x}{\eta_{k_0}}$ with $\eta_{k_0}=pk_0-\omega_{k_0}=k_0(p_z-c)$. Also vectors potential is used to describe the laser field in terms of its plane-wave components, which is essential for understanding the field's interaction with the electron. Now using SFA formalism and the Jacobi-Anger expansion from Equation (4) for linear polarization,

$$\chi_{\mathrm{pL}}(r,t)=\frac{1}{(2\pi)^{\frac{3}{2}}}\sum_{n,m=-\infty}^{\infty}J_n(\rho_L)J_m(\alpha_L)e^{ip_{nm}.r}e^{-i\left(\frac{p^2}{2}+\widetilde{U}_p-(n+2m)\omega_0\right)t}-\mathrm{k_e}\nabla\mathrm{T}\exp(\mathrm{i}\omega_{\mathrm{T}}\mathrm{t}) \tag{6}$$

with the Bessel functions of the first kind $J_i(x)$ and $p_{nm}=p+\frac{\widetilde{U}_p}{\omega_0}-(n+2m)k_0e_z$ and $\widetilde{U}_p=\frac{A_0^2}{4}\frac{\omega_0}{\omega_0-p_zk_0}=\frac{U_p}{1-p_z/c}$ with the ponderomotive energy $U_p=\frac{A_0^2}{4}$. The expansion is essential for describing the electron's quantum state when interacting with a laser field that is linearly polarized, which has significant implications in strong-field physics. The direct transition amplitude is obtained as

$$\mathrm{T}_{\mathrm{pL}}^0=-\frac{i}{(2\pi)^{\frac{1}{2}}}\sum_{n,m=-\infty}^{\infty}J_n(\rho_L)J_m(\alpha_L)V_{nm}(p)\times\delta\left(\frac{p^2}{2}+\widetilde{U}_p(p_z)+I_p-(n+2m)\omega_0\right)-\mathrm{k_e}\nabla\mathrm{T_{nm}}\exp(\mathrm{i}\omega_{\mathrm{T}}\mathrm{t}) \tag{7}$$

where $V_{nm}(p)=\langle p_{nm}|V_{nm}|\phi_0\rangle=-\frac{2^{\frac{3}{4}}I^{\frac{5}{4}}}{\pi}\frac{1}{\frac{p_{nm}^2}{2}+I_p}$ and $I_p=\frac{Z'^2}{2n^2}$ is a matrix element of the Coulomb potential. It is important to note that result Equation (7) recovers the familiar transition amplitude of the dipole strong-field approximation (SFA) in the limit where k→0, which corresponds to neglecting spatial variations in the laser field. By applying delta function properties and solving, we obtain

$$T_p^0 = -\frac{i}{(2\pi)^{\frac{1}{2}}} \sum_{n,m=-\infty}^{\infty} J_n(\rho_L) J_m(\alpha_L) V_{nm}(p) - \mathrm{k_e}\nabla \mathrm{T} \exp(\mathrm{i}\omega_T t) \tag{8}$$

It is crucial for calculating transition probabilities, which are necessary for predicting outcomes in experiments involving strong-field ionization. The DCS is obtained as using Kroll Watson approximation for linear polarization is obtained as

$$\left(\frac{\mathrm{d}\sigma}{d\Omega}\right)_L = \frac{k_f}{k_i} \left| \frac{i}{(2\pi)^{\frac{1}{2}}} \sum_{n,m=-\infty}^{\infty} J_n(\rho_L) J_m(\alpha_L) V_{nm}(\boldsymbol{p}) + \mathrm{k_e}\nabla \mathrm{T} \exp(\mathrm{i}\omega_T t) \right|^2 \tag{9}$$

The DCS is fundamental in characterizing how electrons scatter when subjected to a laser field, which is essential for understanding and predicting experimental results in laser-matter interaction studies. Also for Circular polarization we have $A_c(\boldsymbol{r}, t) = \frac{A_0}{\sqrt{2}}\left(\cos(k_0 r - \omega_0 t) e_x - \sin(k_0 r - \omega_0 t) e_y\right)$ and the derivation for the circularly polarized laser field is similar to the case of linear polarization with the help of Equation (5) with $A(k,t) = Re\{a(k) e^{iu_k}\}$ and $a(k) = \frac{A_0}{\sqrt{2}}\left(e_x + i\Lambda e_y\right)\delta(k - k_0)$, where u(k) = kr − ωt and ω = kc, the wave function for circular polarized is

$$\mathrm{T}_{\mathrm{pL}}^0 \chi_{\mathrm{pC}}(r,t) = \frac{1}{(2\pi)^{\frac{3}{2}}} e^{i\left(\mathrm{p.r} - \frac{p^2}{2}t\right)} e^{-i\Gamma(r,t)} - \mathrm{k_e}\nabla \mathrm{T} \exp(\mathrm{i}\omega_T t) \tag{10}$$

Where $\Gamma(r,t) = \rho_c \sin(u_{k_0} + \Lambda\varphi_p) + 2\alpha_L u_{k_0}$ and Also $\alpha_L = \alpha_c = \frac{A_0^2}{8\eta_{k_0}}, \rho_c = \frac{A_0 psin(v_p)}{\sqrt{2}\eta_{k_0}}$ with $\eta_{k_0} = k_0(p_z - c)$. It is used to model the electron dynamics under circular polarization, which has different symmetry properties compared to linear polarization and leads to distinct interaction outcomes. Use of the Jacobi-Anger expansion, the direct transition amplitude for circular polarization is

$$\mathrm{T}_{\mathrm{pC}}^0 = -\frac{i}{(2\pi)^{\frac{1}{2}}} \sum_{n=-\infty}^{\infty} J_n(\rho_c)\, V_n(\boldsymbol{p}) e^{-in\Lambda\varphi_p} - \mathrm{k_e}\nabla \mathrm{T} \exp(\mathrm{i}\omega_T t) \tag{11}$$

Bessel function plays a key role in determining transition probabilities for ionization processes where the laser field has circular polarization. And DCS for circularized polarized laser field is

$$\left(\frac{\mathrm{d}\sigma}{d\Omega}\right)_C = \frac{k_f}{k_i} \left| \frac{i}{(2\pi)^{\frac{1}{2}}} \sum_{n,=-\infty}^{\infty} J_n(\rho_c)\, V_n(p)\, e^{-in\Lambda\varphi_p} + \mathrm{k_e}\nabla \mathrm{T} \exp(\mathrm{i}\omega_T t) \right|^2 \tag{12}$$

This equation gives the differential cross-section for scattering under circular polarization, analogous to the linear case but tailored for circular polarization's unique characteristics. Understanding this DCS is crucial for experiments and theoretical models involving circular polarization, which has applications in various areas of strong-field and attosecond physics.

3. Results and discussion

3.1. DCS with Linear Polarization laser field

To the study of nature of DCS of developed Equations (9) and (12) with different parameters like temperature, momentum and intensity, the laser intensity 2 a.u. with energy is 1.17 eV are used to analysis all figure mention below. **Figure 1** illustrates the dependence of DCS on temperature for different orbitals in a hydrogen molecule (H_2) under linear polarization. The results show that the DCS increases with rising temperature, with the n = 3 orbital exhibiting a higher DCS compared to the n = 1 orbital. This can be attributed to the differing effects of electron repulsion and the influence of the target nucleus. For the n = 1 orbital, the repulsion between the projected electron and the bound electron is significant due to the proximity of the nucleus. This proximity causes a stronger repulsive interaction between the projected electron and the bound electron, leading to a lower DCS. Conversely, for the n = 3 orbital, the repulsion between the projected electron and the bound electron is less influenced by the nucleus because the bound electron is further from the nucleus. Consequently, the repulsion between the projected and bound electrons is reduced, resulting in a higher DCS.

Figure 1 also demonstrates that as the temperature increases, the DCS rises due to the enhanced oscillatory motion of thermal electrons. The increase in temperature leads to higher thermal energy, which in turn increases the amplitude of electron oscillations. As thermal electrons gain more energy, their oscillatory behavior becomes more pronounced, leading to a higher DCS. This is because the greater energy and amplitude of the thermal electron oscillations contribute more significantly to the scattering cross-section, amplifying the DCS. The temperature dependence of the DCS is influenced by both the electron-nucleus repulsion and the thermal energy of the electrons. At higher temperatures, the increased thermal energy enhances the oscillatory motion of electrons, leading to a higher DCS. Additionally, the effect of electron repulsion varies with the orbital level, with higher orbitals showing a reduced influence from the nucleus and therefore higher DCS values.

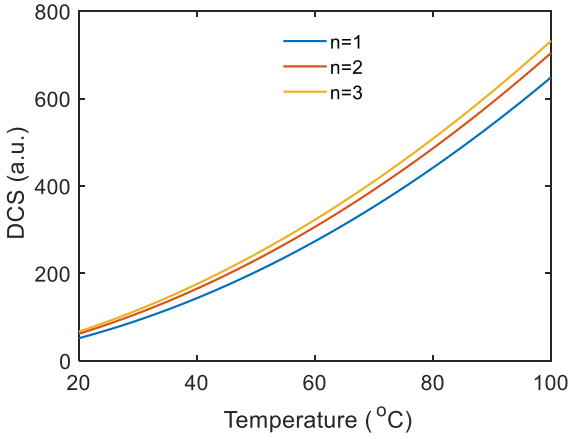

Figure 1. Temperature dependence DCS for linear polarization.

Figure 2 illustrates the variation in DCS with changes in the momentum of

incident thermal electrons at a temperature of 30°C and similar nature was observed at different temperature. The data indicate that the DCS decreases as the energy of the incident thermal electrons increases. The DCS is highest for the $n = 1$ orbital, followed by $n = 2$, and is lowest for $n = 3$. This trend arises because the interaction dynamics between the incident thermal electron and the target atom are influenced by several factors. As the energy of the thermal electron increases, its momentum also increases. This higher momentum results in a greater repulsive interaction between the projected electron and the bound electrons due to the increased kinetic energy of the incident electron. The attraction between the projected electron and the nucleus also plays a role, as higher energy electrons experience a stronger repulsion due to the increased distance from the nucleus.

Furthermore, the DCS varies with the orbital level of the bound electron. For outer orbitals ($n = 2$ and $n = 3$), the repulsion between the projected electron and the bound electron is more pronounced compared to inner orbitals ($n = 1$) as shown in **Figure 2**. In outer orbitals, the higher energy of the projected electron results in a greater repulsive interaction, leading to a lower DCS. In contrast, for the $n = 1$ orbital, where the electron is closer to the nucleus, the repulsive interaction is relatively less, resulting in a higher DCS. In the low-energy region, the DCS is higher compared to the high-energy region. This is because, at lower energies, the interaction time between the projected electron and the bound electron is longer, leading to a more significant repulsive interaction. In contrast, at higher energies, the interaction time is shorter due to the faster movement of the thermal electron, which results in a decreased DCS as the interaction is less prolonged.

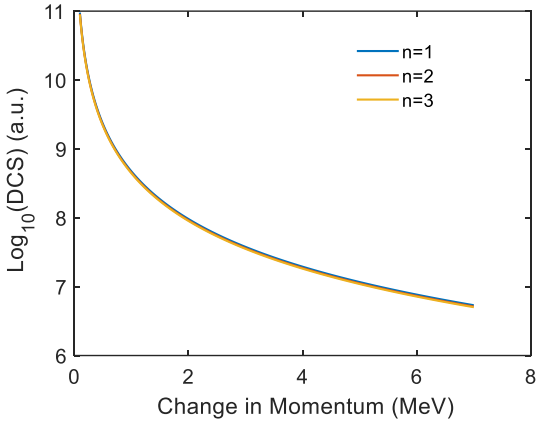

Figure 2. DCS with Change in momentum for linear polarization.

The observed decrease in DCS with increasing incident electron energy can be attributed to the enhanced repulsive interaction at higher energies and the impact of orbital level on the interaction dynamics. Lower-energy regions exhibit higher DCS due to more substantial interaction times and stronger repulsion, whereas higher-energy regions show reduced DCS due to shorter interaction times and decreased repulsion.

Figure 3 depicts the variation in DCS as a function of laser intensity, showing a decrease in DCS with increasing laser intensity. The DCS is higher for the $n = 1$ orbital compared to the $n = 3$ orbital. At lower intensities, the DCS values for different orbitals

are relatively similar. However, as the laser intensity increases, the DCS values for the different orbitals become more distinct, with the n = 1 orbital exhibiting higher DCS and the n = 3 orbital showing lower DCS. This behavior can be attributed to the formation of a dipole in the atom, which is more pronounced for higher orbitals. In higher orbitals, the dipole formation is more significant due to the increased distance between the bound electrons and the nucleus, resulting in a reduced repulsion between the projected and bound electrons. Consequently, the projected electron experiences less repulsion and can approach more closely to the nucleus, leading to a lower DCS.

Conversely, in lower orbitals, the dipole effect is minimal due to the shorter distance between the bound electron and the nucleus. This proximity results in a stronger repulsive interaction between the projected electron and the bound electron. Since the nuclear charge remains constant and the repulsion dominates, the DCS for lower orbitals is higher compared to higher orbitals when subjected to increased laser intensity. Additionally, the excitation of atoms plays a role in this phenomenon. At lower orbital levels, the atom is less excited due to fewer electrons being involved.

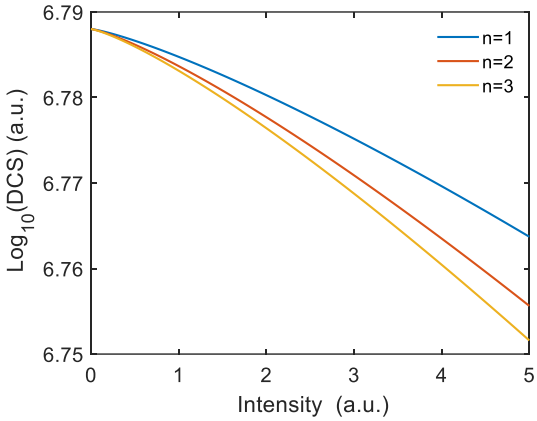

Figure 3. DCS with intensity of laser for linear polarized laser field at 30 °C.

In contrast, higher orbital levels, which have a greater electron density, experience more substantial effects from increased laser intensity. The interaction region for electrons in lower orbitals is more pronounced compared to those in higher orbitals at the same laser intensity. This is because higher electron density in the excited states of higher orbitals results in a more substantial interaction with the laser field, influencing the DCS. The observed decrease in DCS with increasing laser intensity is a result of the complex interplay between dipole formation, repulsive interactions, and atomic excitation. The higher DCS for lower orbitals at higher intensities is due to reduced dipole effects and greater repulsion, while the lower DCS for higher orbitals is due to more significant dipole interactions and increased electron density at higher excitation levels.

3.2. DCS with Circular Polarization laser field

Figure 4 illustrates the DCS as a function of thermal electron temperature for circularly polarized light, which follows a similar trend to that observed for linearly polarized light in **Figure 1**. Specifically, the DCS increases with thermal electron temperature, indicating a similar effect of thermal excitation on electron behavior in

both polarization cases. However, the DCS for circularly polarized light is consistently lower than for linearly polarized light. This discrepancy can be attributed to the differences in the electric field orientation and intensity distribution between linear and circular polarization. For circularly polarized light, the electric field rotates in a helical manner, which leads to a different interaction dynamic compared to the linear polarization where the electric field is oriented along a fixed direction. The helical electric field of circular polarization generally results in a more complex interaction with the thermal electrons, leading to reduced efficiency in transferring energy and momentum compared to linear polarization.

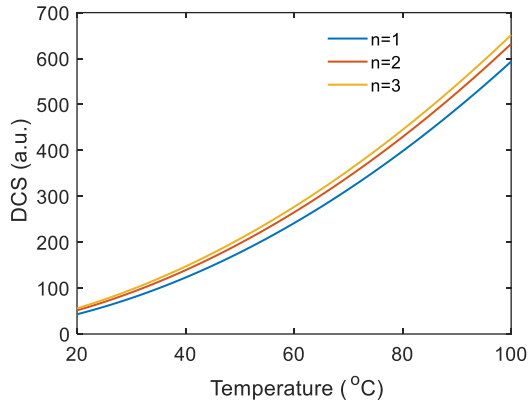

Figure 4. Temperature dependence DCS for circular polarization.

In circular polarization, the varying direction of the electric field can lead to less effective coupling with the electron's motion, resulting in a lower DCS. This reduced interaction efficiency manifests as lower differential cross-sections when compared to linear polarization, where the fixed field direction provides a more consistent and stronger interaction with the electrons. Consequently, while both polarizations show an increase in DCS with thermal electron temperature, the circularly polarized light consistently yields lower DCS values due to its inherent interaction characteristics.

Figure 5 illustrates that the DCS decreases with increasing momentum, with higher orbits exhibiting higher DCS values and lower orbits showing lower values under circular polarization, contrary to linear polarization trends. This discrepancy highlights the significant impact of polarization on electron interactions. Circularly polarized light, with its rotating electric field, can enhance interaction efficiency for higher orbits by better aligning with electron momentum, leading to increased DCS. In contrast, linear polarization's fixed field direction is less effective for aligning with electron motion in higher orbits, resulting in lower DCS values. Therefore, circular polarization generally leads to higher DCS for higher orbits and lower DCS for lower orbits compared to linear polarization.

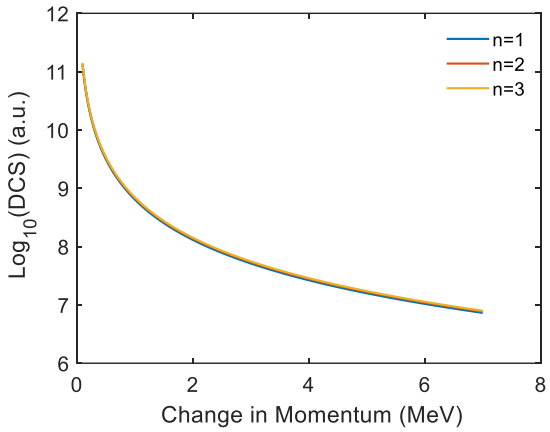

Figure 5. DCS with Change in momentum for circular polarization.

Figure 6 reveals that the DCS decreases with increasing laser intensity for circular polarization at 30°C, exhibiting a pattern similar to linear polarization as shown in **Figure 3**. However, the DCS for circularly polarized light is confined to a narrower range compared to the broader range observed for linear polarization. This narrower range for circular polarization suggests a more focused interaction between the laser and the electrons. The higher DCS observed for circular polarization at the same intensity as linear polarization can be attributed to the more effective coupling of circularly polarized light with the electron's orbital motion. The rotating electric field of circular polarization aligns better with the electron's momentum and enhances interaction efficiency, resulting in higher DCS. Conversely, linear polarization, with its fixed field direction, is less effective in coupling with the electron's motion, leading to a broader but lower DCS range. Thus, circular polarization provides a more concentrated and effective interaction, leading to higher DCS values compared to linear polarization at the same intensity.

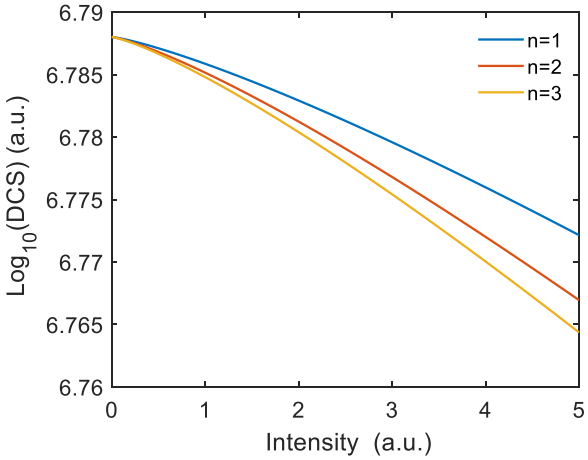

Figure 6. DCS with intensity of laser for circular polarized laser field at 30 °C.

4. Conclusion

The DCS results demonstrate significant variations based on experimental parameters such as temperature, momentum, and laser intensity, as well as the

polarization of the laser field. For linear polarization, the DCS increases with temperature due to enhanced thermal electron oscillations and varying electron repulsion with orbital levels. The DCS is higher for the $n = 3$ orbital compared to $n = 1$, attributed to reduced nuclear repulsion at higher orbitals. As thermal electron energy rises, the DCS decreases due to increased repulsive interactions and shorter interaction times at higher momenta. Laser intensity further influences the DCS, with lower orbitals exhibiting higher DCS values due to stronger repulsive interactions and less dipole effect compared to higher orbitals. In circular polarization, the DCS generally exhibits lower values compared to linear polarization due to less efficient coupling of the rotating electric field with electron motion, despite showing similar temperature dependence. The impact of polarization is evident, with circular polarization enhancing DCS for higher orbitals and narrowing the range of intensity effects. Overall, the results underscore the complex interplay between polarization, temperature, and laser intensity in modulating electron scattering behaviors.

Author contributions: Conceptualization, CS; methodology, CS and SHD; software, SHD; validation, SHD; formal analysis, SHD and NBS; investigation, CS; writing—original draft preparation, CS; writing—review and editing, NBS; supervision, SHD. All authors have read and agreed to the published version of the manuscript.

Conflict of interest: The authors declare no conflict of interest.

References

1. Bunkin FV, Kazakov AE, Fedorov MV. Interaction of intense optical radiation with free electrons (nonrelativistic case). Uspekhi Fizicheskih Nauk. 1972; 107(8): 559–593. doi: 10.3367/ufnr.0107.197208b.0559
2. Faisal FHM. Collision of electrons with laser photons in a background potential. Journal of Physics B: Atomic and Molecular Physics. 1973; 6(11): L312-L315. doi: 10.1088/0022-3700/6/11/003
3. Kroll NM, Watson KM. Charged-Particle Scattering in the Presence of a Strong Electromagnetic Wave. Physical Review A. 1973; 8(2): 804–809. doi: 10.1103/physreva.8.804
4. Bergou J, Varro S. Nonlinear scattering processes in the presence of a quantised radiation field. II. Relativistic treatment. Journal of Physics A: Mathematical and General. 1981; 14(9): 2281–2303. doi: 10.1088/0305-4470/14/9/023
5. Bergou J. Wavefunctions of a free electron in an external field and their application in intense field interactions. I. Non-relativistic treatment. Journal of Physics A: Mathematical and General. 1980; 13(8): 2817–2822. doi: 10.1088/0305-4470/13/8/029
6. Faisal FH. Theory of multiphoton processes. Springer Science & Business Media; 2013.
7. Ehlotzky F, Jaroń A, Kamiński JZ. Electron–atom collisions in a laser field. Physics reports. 1998; 297(2–3), 63–153.
8. Kanya R, Yamanouchi K. Numerical simulation of THz-wave-assisted electron diffraction for ultrafast molecular imaging. Physical Review A. 2017; 95(3). doi: 10.1103/physreva.95.033416
9. Barna IF, Pocsai MA, Varró S. The influence of a strong infrared radiation field on the conductance properties of doped semiconductors. The European Physical Journal Applied Physics. 2018; 84(2): 20101. doi: 10.1051/epjap/2018180156
10. Liang J, Han M, Liao Y, et al. Attosecond-resolved non-dipole photoionization dynamics. Nature Photonics. 2024; 18(4): 311–317. doi: 10.1038/s41566-023-01349-z
11. Böning B, Paufler W, Fritzsche S. Nondipole strong-field approximation for spatially structured laser fields. Physical Review A. 2019; 99(5). doi: 10.1103/physreva.99.053404
12. Rosenberg L, Zhou F. Generalized Volkov wave functions: Application to laser-assisted scattering. Physical Review A. 1993; 47(3): 2146–2155. doi: 10.1103/physreva.47.2146
13. Schafer KJ, Yang B, DiMauro LF, et al. Above threshold ionization beyond the high harmonic cutoff. Physical Review Letters. 1993; 70(11): 1599–1602. doi: 10.1103/physrevlett.70.1599

14. Argüello-Luengo J, Rivera-Dean J, Stammer P, et al. Analog Simulation of High-Harmonic Generation in Atoms. PRX Quantum. 2024; 5(1). doi: 10.1103/prxquantum.5.010328
15. Popruzhenko SV. Coulomb phase in high harmonic generation. Journal of Physics B: Atomic, Molecular and Optical Physics. 2018; 51(14): 144006. doi: 10.1088/1361-6455/aac787
16. Lindsey ML, Bekx JJ, Schlesinger KG, et al. Dynamically assisted nuclear fusion in the strong-field regime. Physical Review C. 2024; 109(4). doi: 10.1103/physrevc.109.044605
17. Mo M, Tamm A, Metsanurk E, et al. Direct observation of strong momentum-dependent electron-phonon coupling in a metal. Science Advances. 2024; 10(11). doi: 10.1126/sciadv.adk9051
18. Urdaneta G, Bak J, Pokharel S, et al. Implementation of Laser Thomson Scattering for Femtosecond Laser-Generated Plasma Channel Characterization. In: Proceedings of the AIAA SCITECH 2024 Forum; 2024. p. 0804.
19. Dhobi SH, Gupta SP, Yadav K, et al. Differential Cross Section with Volkov-Thermal Wave Function in Coulomb Potential. Atom Indonesia. 2024; 1(1): 19–25. doi: 10.55981/aij.2024.1309
20. Titi AS, Drake GWF. Quantum theory of longitudinal momentum transfer in above-threshold ionization. Physical Review A. 2012; 85(4): 041404. doi: 10.1103/physreva.85.041404
21. Milošević DB, Paulus GG, Bauer D, et al. Above-threshold ionization by few-cycle pulses. Journal of Physics B: Atomic, Molecular and Optical Physics. 2006; 39(14): R203–R262. doi: 10.1088/0953-4075/39/14/r01
22. Daněk J, Klaiber M, Hatsagortsyan KZ, et al. Interplay between Coulomb-focusing and non-dipole effects in strong-field ionization with elliptical polarization. Journal of Physics B: Atomic, Molecular and Optical Physics. 2018; 51(11): 114001. doi: 10.1088/1361-6455/aaba42
23. Peshkov AA, Seipt D, Surzhykov A, et al. Photoexcitation of atoms by Laguerre-Gaussian beams. Physical Review A. 2017; 96(2). doi: 10.1103/physreva.96.023407